



CHORUS

This is the accepted manuscript made available via CHORUS. The article has been published as:

## Demixing Instability in Dense Molten $\text{MgSiO}_3$ and the Phase Diagram of MgO

Brian Boates and Stanimir A. Bonev

Phys. Rev. Lett. **110**, 135504 — Published 26 March 2013

DOI: [10.1103/PhysRevLett.110.135504](https://doi.org/10.1103/PhysRevLett.110.135504)

# Demixing instability in dense molten $\text{MgSiO}_3$ and the phase diagram of $\text{MgO}$

Brian Boates,<sup>1,2</sup> and Stanimir A. Bonev<sup>1,2</sup>

<sup>1</sup>*Department of Physics, Dalhousie University,*

*Halifax, NS B3H 3J5, Canada and*

<sup>2</sup>*Lawrence Livermore National Laboratory, Livermore, CA 94550, USA*

## Abstract

The phase diagrams of  $\text{MgSiO}_3$  and  $\text{MgO}$  are studied from first-principles theory for pressures and temperatures up to 600 GPa and 20,000 K. Through evaluation of finite-temperature Gibbs free energies, using both DFT-GGA and hybrid exchange-correlation functionals, we find evidence for a vast pressure-temperature regime where molten  $\text{MgSiO}_3$  decomposes into liquid  $\text{SiO}_2$  and solid  $\text{MgO}$ , with a volume change of approximately 1.2 percent. The demixing transition is driven by the crystallization of  $\text{MgO}$  – the reaction only occurs below the high-pressure  $\text{MgO}$  melting curve. The predicted transition pressure at 10,000 K is in close proximity to an anomaly reported in recent laser-driven shock experiments of  $\text{MgSiO}_3$ . We also present new results for the high-pressure melting curve of  $\text{MgO}$  and its B1-B2 solid phase transition, with a triple point at 364 GPa and 12,000 K.

PACS numbers: 62.50.-p, 02.70.-c, 61.20.Ja, 91.45.-c

The evolution and structure of terrestrial planetary interiors depend largely on the thermodynamic stability of the mantle minerals that compose them [1–3]. In particular, the phases and decomposition of magnesium silicate ( $\text{MgSiO}_3$ ) at the pressure ( $P$ ) and temperature ( $T$ ) conditions found in the Earth’s mantle, as well as in Earth-like and Saturn-like exoplanets, have been a subject of great interest [4–14]. Most studies to date have focused on the crystallographic transformations of  $\text{MgSiO}_3$ -perovskite and post-perovskite solids. However, recent shock compression experiments reported discontinuous phase changes in liquid  $\text{MgSiO}_3$  with a  $6.3 \pm 2.0$  percent volume change [15]. While the conditions where these changes take place lie outside the pressure-temperature range found within the Earth, such transitions could play an important role during the giant impacts that lead to planetary formation. They would also have serious implications for the convection mechanisms in the primitive stages of the Earth mantle’s development, as well as geophysical processes in the interiors of extra-solar super-Earths.

The observed anomalies in molten  $\text{MgSiO}_3$  were interpreted as a first-order liquid-liquid phase transition (LLPT) [15]. LLPT’s are exceptionally rare in equilibrium liquids and have only been reported for a few systems [16–19]. In all known cases, they are driven by drastic changes in the bonding properties – metallization (except for  $\text{CO}_2$ ) and/or polymerization. However, no electrical anomalies or significant changes in the nature of the chemical bonding in liquid  $\text{MgSiO}_3$  are expected at the reported conditions ( $T > 8,000$  K and  $P > 300$  GPa). Therefore, in addition to being highly relevant for planetary science, understanding the high-pressure phase diagram of  $\text{MgSiO}_3$  addresses the fundamental question of whether a LLPT could exist at extreme temperatures where the importance of ion kinetics is comparable to that of the chemical interactions.

In this Letter, we report on an investigation of liquid  $\text{MgSiO}_3$  from first-principles theory. The problem at hand requires computing the free energies of  $\text{MgSiO}_3$  and its possible reaction products. For the high temperatures of interest, entropic contributions are expected to play an important role and must be determined with high accuracy. We have also taken special care to assess the validity of the employed exchange-correlation approximations, which is necessary at extreme compression [20, 21] or when comparing phases with significantly different electronic properties. Our results confirm that liquid  $\text{MgSiO}_3$  becomes thermodynamically unstable under compression. However, despite the excellent agreement found here with the measured transition pressure at 10,000 K, our explanation for the instability is en-

tirely different. In what follows, we show that liquid  $\text{MgSiO}_3$  undergoes a phase separation into solid magnesium oxide and liquid silica.

We have performed first-principles molecular dynamics (FPMD) simulations (at constant number of particles  $N$ , volume  $V$ , and temperature  $T$ ) of liquid and solid  $\text{MgSiO}_3$ ,  $\text{MgO}$ , and  $\text{SiO}_2$  up to pressures ( $P$ ) and temperatures of 600 GPa and 20,000 K. Calculations were carried out using finite- $T$  density functional theory (DFT) [22] within the Perdew-Burke-Ernzerhof [23] generalized gradient approximation (PBE-GGA) using the Vienna *ab initio* Simulation Package (*VASP*) [24]. We used Born-Oppenheimer dynamics, a Nosé-Hoover thermostat, and a  $\Gamma$ -point sampling of the Brillouin zone for all simulations. Supercells of 135 atoms were used for simulations of liquid  $\text{MgSiO}_3$ , 96 atoms for liquid  $\text{SiO}_2$ , and 100 atoms for liquid  $\text{MgO}$ , as well as 64 and 128-atom supercells for simulations of the B1 and B2 solid phases of  $\text{MgO}$ , respectively. Changes to the free energies were negligible when using up to 216 and 256-atom supercells for the B1 solid and liquid phases of  $\text{MgO}$ , while also maintaining good agreement with pair correlation functions given in ref. 25.

For each system, convergence with respect to  $\mathbf{k}$ -point sampling was checked using up to a  $4 \times 4 \times 4$  grid on FPMD snapshots to ensure the desired level of accuracy (few meV/atom). At each  $P$  and  $T$ , simulations were equilibrated for 1-2 ps and run for an additional 5-10 ps (necessary for a well-converged vibrational spectra) with a 0.75 fs time-step. We employed an 8-electron projector augmented wave (PAW) pseudopotential (PP) with a 2.00 Bohr core radius for Mg atoms, a 4-electron PAW PP with a 1.50 core radius for Si atoms, and a 6-electron PAW PP with a 1.10 core radius for O atoms. All calculations were performed with an 875 eV plane-wave cut-off energy.

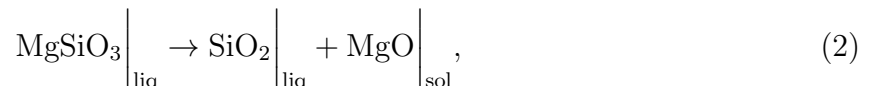
Finite- $T$  Gibbs free energies were computed using ensemble (time) averages of energies, pressures, and temperatures from FPMD simulations. Entropies were calculated using vibrational spectra calculated via Fourier transform of the velocity auto-correlation functions (VACF) obtained from simulation trajectories. For liquid phases, this was done following the method prescribed in ref. 26 where the vibrational spectrum is decomposed into gas and solid-like parts. This method has been used to successfully predict demixing transitions in dense liquid alloys, accurate to within 1-2 % of thermodynamic integration free energies [27]. The Gibbs free energy of mixing is calculated as  $\Delta G_{\text{mix}} = G_{\text{MgSiO}_3} - (2/5)G_{\text{MgO}} - (3/5)G_{\text{SiO}_2}$ . Here  $G_X$  is the free energy per atom of species  $X$ , where  $X$  is  $\text{MgSiO}_3$ ,  $\text{MgO}$ , or  $\text{SiO}_2$ .

It is well known that standard DFT functionals possess an incorrect bias toward metal-

lic systems. Given that we are interested in transitions between metallic (the liquids) and insulating (the solids) mineral phases, we have included corrections for each phase of each material considered for a variety of  $P$ - $T$  conditions using the Heyd-Scuseria-Ernzerhof (HSE) hybrid functional [28]. This was done at the level of thermodynamic perturbation by recalculating the energies of atomic configurations obtained from FPMD using the HSE functional. The resulting corrections to the free energies of mixing are on the order of tens of meV/atom. It is important to note that the hybrid functional does not qualitatively affect our conclusions, but rather results in small changes to transition pressures and temperatures. Similarly, tests employing a van der Waals density functional (vdW-DF) [29] led to fairly small changes in free energies of mixing ( $< 10$  meV/atom), which have been neglected here.

The properties of molten  $\text{MgSiO}_3$ , are studied along the 10,000 and 16,000 K isotherms for pressures up to 600 GPa. An exhaustive analysis of static and dynamic structural properties reveals no notable or discontinuous changes with pressure. Furthermore, the pressures and energies obtained from simulation averages are smooth functions of the  $V$ . Should there be a volume change of 6.3 % as reported in ref. 15, one would expect a distinct plateau in  $P(V)$ , which we do not see in our data.

The decomposition reactions of  $\text{MgSiO}_3$  that we consider, namely:



require knowledge of the Gibbs free energies and phase boundaries of MgO and  $\text{SiO}_2$ . While  $\text{SiO}_2$  is well known to be liquid under the conditions of interest for these reactions [36], MgO has solid-liquid and solid-solid phase lines in close proximity [32]. Therefore, in order to properly evaluate the Gibbs free energy of mixing for  $\text{MgSiO}_3$ , we have determined the high-pressure phase boundaries between liquid MgO and its B1 (NaCl-type) and B2 (CsCl-type) solid phases using their finite- $T$  Gibbs free energies. These results are summarized in a new MgO phase diagram, presented in Fig. 1. The free energies of liquid MgO and its B1 and B2 solid phases are shown along the 10,000 K isotherm in Fig. 1 (inset). We have presented results from PBE-GGA, as well as with corrections to the energies using the HSE hybrid functional, as discussed above. Our melting temperatures are slightly higher than those previously predicted [31–33]. To our knowledge, these are the first calculations of the MgO melting curve that employ a hybrid functional, which is partially responsible

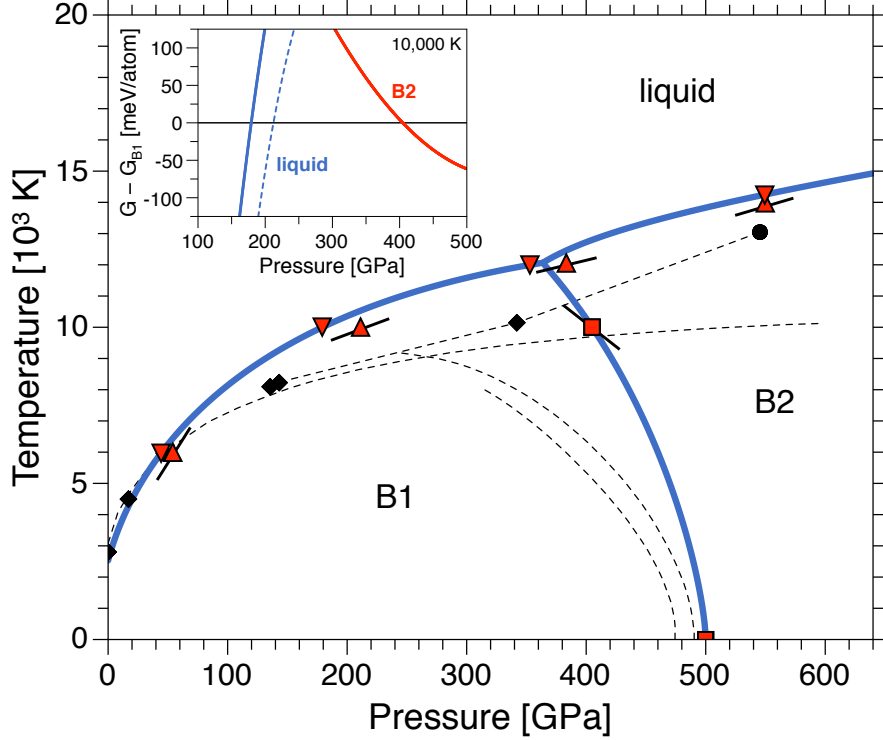


FIG. 1. High-pressure phase diagram of MgO revealed by first-principles free energy calculations. Red triangles show our melting points for B1 and B2 phases obtained with (downward) and without (upward) HSE corrections to the free energies. Our predicted B1-B2 transition points are given by red squares. Short black lines underneath our data represent Clausius-Clapeyron slopes. Thick blue lines are Kechin fits to our HSE-corrected data [30], which give rise to a triple point at 364 GPa and 12,000 K. Previous theoretical predictions of B1 (diamonds) and B2 (circle) melting points are also shown [31, 32]. Black dashed lines indicate theorized high-pressure melting curves [32, 33] as well as B1-B2 phase boundaries [32, 34, 35]. Inset: Gibbs free energies for MgO phases relative to the B1 phase along the 10,000 K isotherm with (solid lines) and without (dashed lines) HSE corrections.

for our higher melting temperatures; regular DFT functionals incorrectly favor the metallic fluid over the insulating B1 and B2 solids. The B1-B2 transition found here at 405 GPa and 10,000 K, as well as the zero-temperature transition at 500 GPa are in good agreement with previous work [32, 34, 35]. The Clausius-Clapeyron slopes for our B1-liquid transition points are 61.0 K/GPa at 6,000 K, 14.0 K/GPa at 10,000 K, and 8.9 K/GPa at 12,000 K, while the slope at the B2-liquid transition is 12.3 K/GPa at 14,000 K and the B1-B2 transition slope is -30.4 K/GPa at 10,000 K. By fitting the melting curves and the solid-solid phase line with a

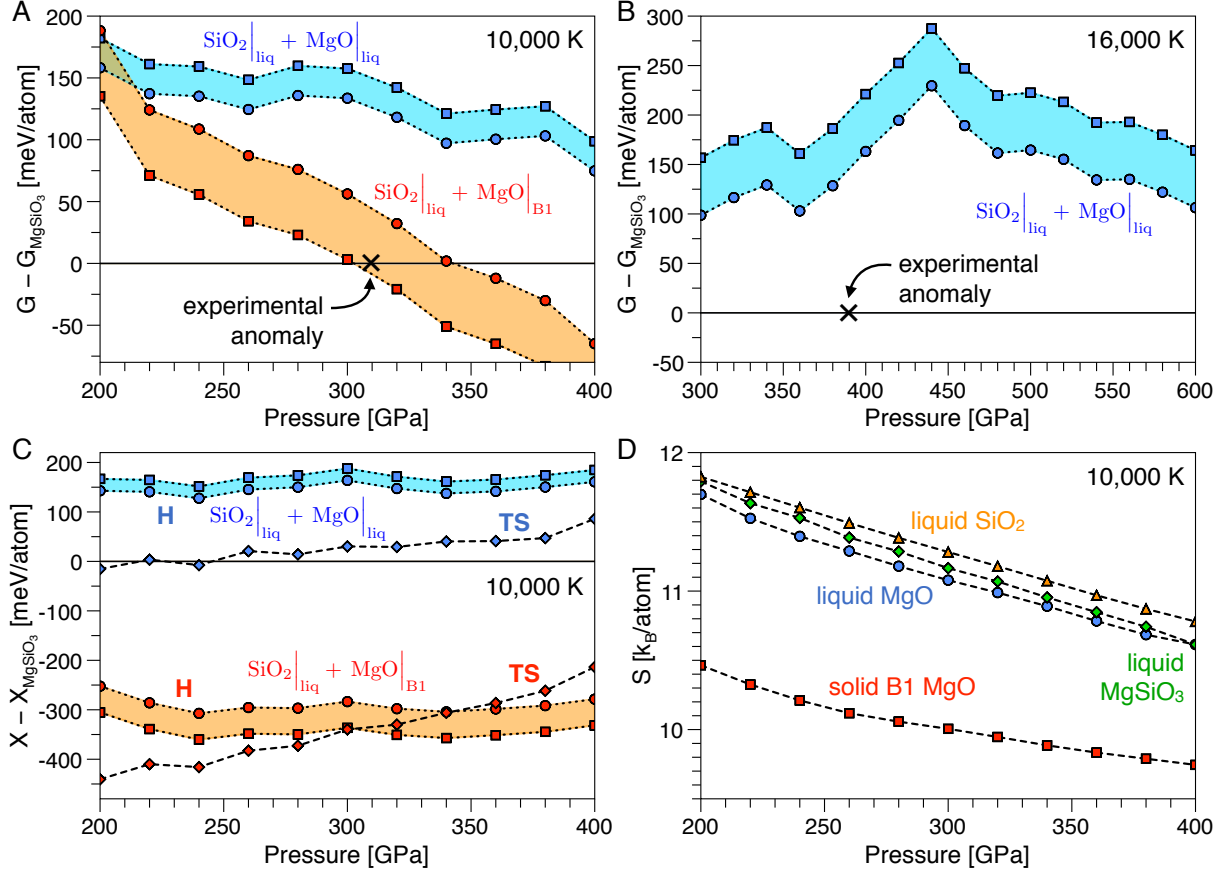


FIG. 2. Gibbs free energies of mixing along the (a) 10,000 and (b) 16,000 K isotherms computed using MgO liquid (blue) and MgO solid B1 (red) with (squares) and without (circles) HSE corrections. Anomalies measured in shocked MgSiO<sub>3</sub> are given by black crosses. (c) Enthalpy and entropy (diamonds) contributions to the Gibbs free energies of mixing at 10,000 K. (d) Total entropies of the various phases considered at 10,000 K.

Kechin equation [37], we obtain the B1-B2-liquid triple point at 364 GPa and 12,000 K. An estimate for the Clausius-Clapeyron slope at the triple point yields 22.9 K/GPa, consistent with 23.4 K/GPa obtained through direct differentiation of our B2-liquid Kechin equation-fitted boundary.

Having determined the high-pressure MgO phase diagram we proceeded to compute the Gibbs free energies of mixing associated with reactions (1) and (2). Fig. 2 shows these results for the 10,000 and 16,000 K isotherms with and without HSE corrections. At both 10,000 and 16,000 K we find that reaction (1) is not exothermal. However, calculations at 10,000 K indicate that demixing reaction (2) must occur above 303 GPa, and it is the crystallization

of MgO taking place at lower temperatures that drives the phase separation process in liquid MgSiO<sub>3</sub>. In Fig. 2(c), we show the enthalpy and entropy contributions to the Gibbs free energies of mixing at 10,000 K. As expected, the presence of solid MgO in reaction (2) results in a largely negative enthalpy of mixing, but also contributes considerably less to the entropy of the products, as seen in Fig. 2(d). Upon compression, the entropy of mixing continues to increase gradually, while the enthalpy of mixing remains relatively flat. At 303 GPa the two terms cross, giving rise to the demixing of fluid MgSiO<sub>3</sub> via reaction (2). Fig. 2(c) also shows the enthalpy and entropy of mixing for reaction (1). Again, the enthalpy of mixing is relatively flat (this time, positive) over the entire pressure range, while the entropy of mixing is nearly zero and rises too slowly to induce the demixing process given by (1) at these pressures. The total entropies for each phase at 10,000 K are shown in Fig. 2(d). As expected, solid B1 MgO possesses lower entropy than the liquids, however, its entropy decreases at the slowest rate with pressure; this is directly responsible for the demixing of molten MgSiO<sub>3</sub>.

To determine the phase line associated with demixing reaction (2), we performed simulations at 500 GPa. At this pressure, our free energy calculations indicate liquid MgSiO<sub>3</sub> becomes thermodynamically unstable below 12,000 K, where it decomposes into liquid SiO<sub>2</sub> and solid B2 MgO. Our results are summarized in a new high-pressure liquid phase diagram for MgSiO<sub>3</sub>, shown in Fig. 3. We have highlighted a large region in  $P$ - $T$  space spanning hundreds of gigapascals and thousands of degrees Kelvin between the MgSiO<sub>3</sub> and MgO melting curves, where our calculations indicate that molten MgSiO<sub>3</sub> decomposes into solid MgO and liquid SiO<sub>2</sub>. As before, our transition points are shown with and without HSE corrections to the energies to account for any metallic bias. The Clausius-Clapeyron slopes for the demixing reactions involving the B1 and B2 phases of MgO are 11.1 and 18.9 K/GPa, respectively, fairly consistent with the locations of each point relative to one another.

Given how close our 10,000 K transition pressure is to the anomaly measured in ref. 15, we propose that the experimental findings at these conditions are indeed a signature of the phase separation predicted here. However, our demixing transition near 400 GPa takes place at much lower temperature than the experimental anomaly. In order to understand the significance of this disagreement, we have considered the amount of error in our calculations needed to give rise to a demixing reaction that coincides with the anomaly measured at 16,000 K and 390 GPa. Based on the data presented in Fig. 2(b), we estimate that an

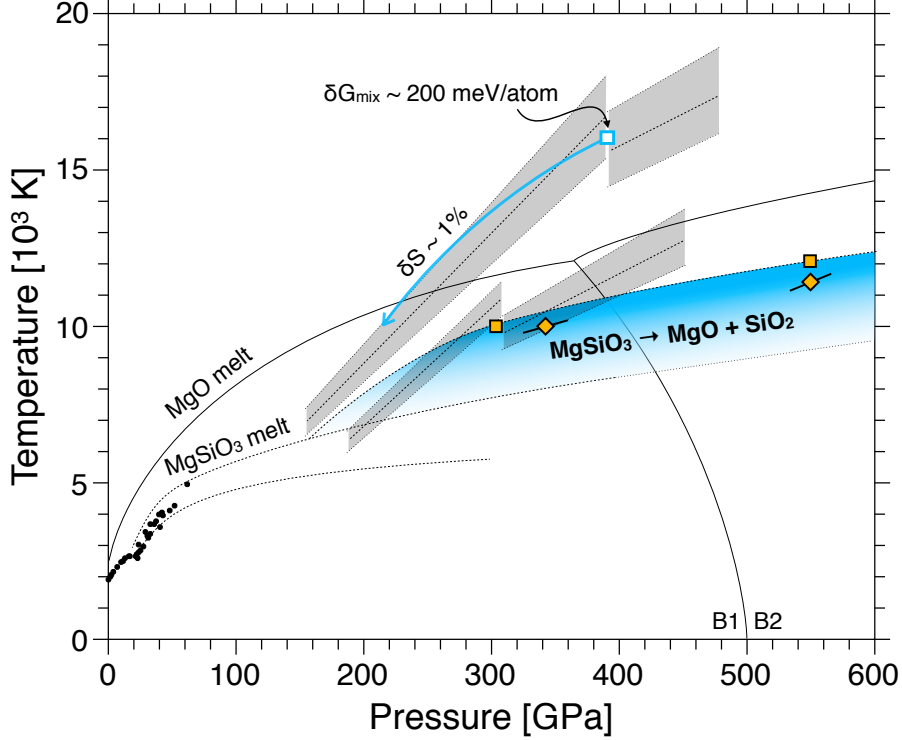


FIG. 3. Proposed high-pressure phase diagram of liquid  $\text{MgSiO}_3$ . The shaded blue region shows the  $P$ - $T$  region where liquid  $\text{MgSiO}_3$  phase separates into solid  $\text{MgO}$  and liquid  $\text{SiO}_2$ . Demixing transition points were calculated with (squares) and without (diamonds) HSE energy corrections. The short black lines underneath our data represent Clausius-Clapeyron slopes. Recent shock measurements are shown with shaded grey regions [15]. The blue square indicates the demixing transition pressure for reaction (1) assuming a systematic 200 meV/atom error in our Gibbs free energy calculations, equivalent to approximately 1% error in the evaluation of our total entropies. The blue arrow forms the corresponding demixing phase boundary (guide to the eye) taking into account such a systematic error. Previous theoretical [33, 38] and experimental [39, 40] results for the  $\text{MgSiO}_3$  melting curve are shown by black dashed lines and black dots, respectively.  $\text{MgO}$  phase boundaries presented in Fig. 1 are given by solid black lines for comparison.

error of approximately 200 meV/atom in  $\Delta G_{\text{mix}}$  would be required. The biggest source of uncertainty in our calculations is the entropy. A 200 meV/atom error in  $\Delta G_{\text{mix}}$  translates to about 1% of the total entropy at 16,000 K. A corresponding 1% systematic error in the total entropies at 10,000 K would shift the demixing transition by approximately 105 meV/atom. If we accept such a *systematic* error, the 10,000 K demixing pressure would be lowered

to 215 GPa, indicated by the blue arrowhead in Fig. 3. The curvature of the blue arrow between the hypothetical 16,000 and 10,000 K transition points is a guide to the eye, meant to represent a contour of 1% error in total entropy. While the authors appreciate that such large qualitative differences may arise from small uncertainties, it is virtually unavoidable at these temperatures; free energies checked using state-of-the-art thermodynamic integration methods at one  $P$ - $T$  point yield results within 1-2% of the method employed in this work. However, because we do not observe significant variations in the liquid structure for the  $P$ - $T$  conditions of interest, any computational errors would likely be systematic, making it difficult to justify the experimental observations at both temperatures simultaneously.

The results presented here provide a broad characterization of the MgO and MgSiO<sub>3</sub> phase diagrams up to 600 GPa and 20,000 K. Our first-principles simulations of liquid MgSiO<sub>3</sub> show no rapid or discontinuous changes in its structural, electronic, or thermodynamic properties over the entire range of experimental  $P$ - $T$  conditions. Instead, we predict an expansive region between MgSiO<sub>3</sub> and MgO melting curves, in which molten MgSiO<sub>3</sub> decomposes into solid MgO and liquid SiO<sub>2</sub>. Similar phase separation of MgSiO<sub>3</sub> into MgO and SiO<sub>2</sub> has been previously predicted in its solid phases, albeit at considerably higher pressures [11]. Moreover, a decomposition to MgSi<sub>2</sub>O<sub>5</sub> and MgO has also been predicted for solid MgSiO<sub>3</sub> [13] between  $\sim$  1-2 terapascals. We have also considered these products in the fluid and find their free energy to be competitive for the  $P$ - $T$  conditions considered, but never the lowest (see Supplementary Material). The demixing transition predicted here may have played a significant role in the primitive mantle, contributing to the large amounts of MgO and SiO<sub>2</sub> present today. An accurate description of these mantle minerals at high pressures and temperatures is of the utmost importance in understanding terrestrial planetary formation as well as the evolution of their interiors.

We wish to thank E. Schwegler, A.M. Teweldeberhan, and S. Hamel for discussions. This work was supported by the Lawrence Livermore National Laboratory (LLNL), the Natural Sciences and Engineering Research Council of Canada (NSERC), and the Killam Trusts. Computational resources were provided by the Canadian foundation for Innovation, ACEnet, WestGrid, and LLNL. The work at LLNL was performed under the auspices of the US Department of Energy under contract No. DE-AC52-07NA27344.

- 
- [1] F. Birch, *J. Geophys. Res.*, **57**, 227 (1952).
- [2] T. Ahrens, D. Anderson, and A. Ringwood, *Rev. Geophys.*, **7**, 667 (1969).
- [3] U. Christensen, *Annu. Rev. Earth Planet. Sci.*, **23**, 65 (1995).
- [4] C. Meade, H.-K. Mao, and J. Hu, *Science*, **268**, 1743 (1995).
- [5] S. Saxena, L. Dubrovinsky, P. Lazor, Y. Cerenius, P. Haggkvist, M. Hanfland, and J. Hu, *Science*, **274**, 1357 (1996).
- [6] G. Serghiou, A. Zerr, and R. Boehler, *Science*, **280**, 2093 (1998).
- [7] S.-H. Shim, T. Duffy, and G. Shen, *Science*, **293**, 2437 (2001).
- [8] M. Murakami, K. Hirose, K. Kawamura, N. Sata, and Y. Ohishi, *Science*, **304**, 855 (2004).
- [9] A. Oganov and S. Ono, *Nature*, **430**, 445 (2004).
- [10] L. Stixrude and B. Karki, *Science*, **310**, 297 (2005).
- [11] K. Umemoto, R. Wentzkovitch, and P. Allen, *Science*, **311**, 983 (2006).
- [12] S. Lee, J.-F. Lin, Y. Cai, N. Hiraoka, P. Eng, T. Okuchi, H.-K. Mao, Y. Meng, M. Hu, P. Chow, J. Shu, B. Li, H. Fukui, B. Lee, H. Kim, and C.-S. Yoo, *Proc. Nat. Acad. Sci.*, **105**, 7925 (2008).
- [13] K. Umemoto and R. Wentzkovitch, *Earth Planet. Sci. Lett.*, **311**, 2011 (2011).
- [14] M. Murakami and J. Bass, *Proc. Nat. Acad. Sci.*, **108**, 17286 (2011).
- [15] D. Spaulding, R. McWilliams, R. Jeanloz, J. Eggert, P. Celliers, D. Hicks, G. Collins, and R. Smith, *Phys. Rev. Lett.*, **108**, 065701 (2012).
- [16] Y. Katayama, T. Mizutani, W. Utsumi, O. Shimomura, M. Yamakata, and K. Funakoshi, *Nature*, **403**, 170 (2000).
- [17] B. Boates and S. Bonev, *Phys. Rev. Lett.*, **102**, 015701 (2009).
- [18] M. Morales, C. Pierleoni, E. Schwegler, and D. Ceperley, *Proc. Nat. Acad. Sci.*, **107**, 12799 (2010).
- [19] B. Boates, A. Teweldeberhan, and S. Bonev, *Proc. Nat. Acad. Sci.*, **109**, 14808 (2012).
- [20] A. Teweldeberhan, J. Dubois, and S. Bonev, *Phys. Rev. Lett.*, **105**, 235503 (2010).
- [21] A. Teweldeberhan, J. Dubois, and S. Bonev, *Phys. Rev. B*, **86**, 064104 (2012).
- [22] P. Hohenberg and W. Kohn, *Phys. Rev.* **136**, B864 (1964); W. Kohn and L. Sham, *Phys. Rev.* **140**, A1133 (1965).

- [23] J. Perdew, K. Burke, and M. Ernzerhof, *Phys. Rev. Lett.*, **77**, 3865 (1996).
- [24] G. Kresse and J. Hafner, *Phys. Rev. B* **47**, 558 (1993); G. Kresse and X. Furthmuller, *Comp. Mat. Sci.* **6**, 15 (1996).
- [25] A. Aguado and P. Madden, *Phys. Rev. Lett.*, **94**, 068501 (2005).
- [26] S.-T. Lin, M. Blanco, and W.A. Goddard III, *J. Chem. Phys* **119**, 11792 (2003); S.-T. Lin, P.K. Maiti, and W.A. Goddard III, *J. Phys. Chem. B* **114**, 8191 (2010).
- [27] A. Teweldeberhan and S. Bonev, *Phys. Rev. B*, **83**, 134120 (2011).
- [28] J. Heyd, G. Scuseria, and M. Ernzerhof, *J. Chem. Phys.*, **121**, 2780 (2003).
- [29] M. Dion, H. Rydberg, E. Schroder, D. Langreth, and B. Lundqvist, *Phys. Rev. Lett.*, **92**, 246401 (2004).
- [30] Kechin fit parameters for B1 melting curve:  $P_0 = 0$  GPa,  $T_0 = 2533$  K,  $a_0 = 8.71$  GPa,  $a_1 = 0.495$ ,  $a_2 = 0.000816$  GPa $^{-1}$ . B2 melting curve:  $P_0 = 363.5$  GPa,  $T_0 = 12060.0$  K,  $a_0 = 40.6$  GPa,  $a_1 = 0.0690$ ,  $a_2 = -0.000259$  GPa $^{-1}$ . B1-B2 phase boundary:  $P_0 = 500$  GPa,  $T_0 = 100$  K,  $a_0 = -0.0929$  GPa,  $a_1 = 0.684$ ,  $a_2 = -0.00145$  GPa $^{-1}$ .
- [31] D. Alfe, *Phys. Rev. Lett.*, **94**, 235701 (2005).
- [32] A. Belonoshko, S. Arapan, R. Martonak, and A. Rosengren, *Phys. Rev. B*, **81**, 054110 (2010).
- [33] N. de Koker and L. Stixrude, *Geophys. J. Int.*, **178**, 162 (2009).
- [34] A. Oganov, M. Gillan, and G. Price, *J. Chem. Phys.*, **118**, 10174 (2003).
- [35] Z. Wu, R. Wentzcovitch, K. Umemoto, B. Li, K. Hirose, and J.-C. Zheng, *J. Geophys. Res.*, **113** (2008).
- [36] D. Hicks, T. Boehly, J. Eggert, J. Miller, P. Celliers, and G. Collins, *Phys. Rev. Lett.*, **97**, 025502 (2006).
- [37] V. Kechin, *J. Phys. Condens. Matter*, **7**, 531 (1995).
- [38] A. Belonoshko, N. Skorodumova, A. Rosengren, R. Ahuja, B. Johansson, L. Burakovsky, and D. Preston, *Phys. Rev. Lett.*, **94**, 195701 (2005).
- [39] F. Boyd, J. England, and B. Davis, *J. Geophys. Res.*, **69**, 2101 (1964).
- [40] A. Zerr and R. Boehler, *Science*, **262**, 553 (1993).